Tliha Mohamed (Orcid ID: 0000-0001-7329-1441)

Electrochemical study of $LaGaO_3$ as novel electrode material of hydrogen battery (Ni/MH)

M. Tliha[a,b,*], A.Kaabi[a], C. Khaldi[a], A. Dhahri[c], N. Fenineche[d], O. ElKedim[e], J. Lamloumi[a]

[a]*Department of Physics,University Faculty,Umm-Alqura University, Al-Qunfudah, Saudi Arabia*

[b]*University of Tunis, laboratory of Mechanics, Materials and Processes, group of metal hydrides, ENSIT (Ex ESSTT), Tunis, Tunisia*

[c]*University of Monastir, laboratory of Physical Chemistry of Materials, Monastir, Tunisia*

[d]*ICB-LERMPS/FR FCLAB, UTBM, Site de Sévenans, 90010 Belfort Cedex, France.*

[e]*FEMTO-ST, MN2S, UTBM, Site de Sévenans, 90010 Belfort Cedex, France.*

Abstract

The physico-chemical performance of the novel anode $LaGaO_3$ for Ni/MH accumulators was studied using electrochemical impedance spectroscopy (EIS) method during cycling. The measured EIS data of the perovskite oxide is fitted according to the proposed equivalent circuit representing various processes involved in the mechanism of hydrogenation/dehydrogenation reactions of the oxide. Different kinetic elements such as current density I_0, charge transfer resistance R_{ct}, hydrogen transfer resistance R_{ht}, double layer capacitance C_{dl} and mass hydrogen diffusion Y_0 were estimated under cycling. The EIS results relieved that current density I_0 of the oxide increase quickly during the activation process and its maximum value is obtained at the second cycle (377.67 mA g^{-1}). The degradation of the charge transfer rate of the oxide after activation can be ascribed to the corrosion of the electrode/electrolyte interface. The variation of the Warburg impedance Y_0 could be attributed to the change in the morphological and the structure of the working

This article has been accepted for publication and undergone full peer review but has not been through the copyediting, typesetting, pagination and proofreading process which may lead to differences between this version and the Version of Record. Please cite this article as doi: 10.1002/ep.13930

electrode over cycling. The EIS analysis relieved that electrochemical behavior of the oxide is controlled by the charge-transfer rate and the modification of the electrode surface.

Keywords: Ni/MH battery, Electrochemical properties, EIS method, Hydrogen storage

* Corresponding author: M. Tliha: matliha@uqu.edu.sa/mtliha@gmail.com

1. Introduction

The characteristics of active compounds, applied as anodes for the commercialized nickel-metal (Ni/MH) hydrogen battery, have a significant impact on the physico-chemical hydrogenation performance of the battery [1-5]. The AB_5-type intermetallic alloys are often used as anode materials in the commercial (Ni/MH) hydrogen battery due to their good electrochemical performance [6-19]. However, the limited reversible capacity and high cost of these intermetallic compounds prevent their practical application in the commercial hydrogen battery. Therefore, considerable studies have been carried to improve the kinetic behavior of the MH anode. Recently, perovskite oxides ABO_3 are considered as innovative anode candidates for hydrogen batteries systems [20-24]. These oxides have been received a great interest in the recent years because of their good hydrogen storage properties and high discharge capacity compared with traditional metal hydrides.

Among the electrochemical methods, The EIS method is a powerful tool to study the electrode/electrolyte interface because it allows distinguishing various processes involved in the mechanism of hydrogenation/dehydrogenation reactions of metal hydrides (MH) electrodes [25-27]. A very few investigations about the kinetic properties of the perovskite oxides using electrochemical impedance spectroscopy (EIS) method are presented. In our recently published [28], the $LaGaO_3$ perovskite oxide was reported as a potential negative material for Ni/MH battery. However, the kinetic characteristic of the aforementioned oxide has never been researched until now using EIS.

In the present study, we examine the EIS behavior of this $LaGaO_3$ electrode during cycling and interpreted the EIS by an physico-chemical model based in the experimental results. The effect of charge/discharge cycling on the kinetics parameters characterizing various processes on the electrode surface is discussed.

2. Experimental

The $LaGaO_3$ electrode oxide was prepared by the conventional sol-gel technique. The preparation process of this oxide compound and their structural characterization were presented in our previous work [28]. The obtained XRD result shows that the $LaGaO_3$ electrode crystallizes in the orthorhombic structure with Pnma space group. The $LaGaO_3$ sample was constructed, using the so-called the "latex" method [29,30], as a mixture of 60 wt% $LaGaO_3$ powder, 20 wt% carbon black to ensure the best electrode conductivity and 20 wt polytetrafluoroethylene (PTFE) to make the electrode more elasticity. Two pieces of 0.5 cm^2 of this mixture was compressed on each side of a nickel grid, which played the role of a current collector [31,32]. The electrochemical impedance spectroscopy for the working oxide was tested at 328 K, using a Potentiostat-Galvanostat system with a conventional open three-electrode cell, consisting of a $LaGaO_3$ working electrode, a Hg/HgO reference electrode, a gold wire counter electrode. The electrolyte was 1 M KOH solution.

The impedance measurements were realized at 100% state of charge for 18 charge/discharge cycles. The EIS spectra of the oxide were collected in the frequency range from 1 mHz to 1000 kHz with an AC amplitude perturbation of 5 mV vs. the equilibrium potential. The measured EIS data of the oxide is fitted according to the proposed equivalent circuit using the software ZSimpWin 3.1.

3. Results and discussion

The behavior of the anode material is mainly governed by the rate of the hydrogen diffusion process and/or the kinetic of the hydriding/dehydriding reaction taking place on the

electrode/electrolyte interface. The EIS is an important and a robust diagnosis electroanalytical technique used for investigating the electrochemical properties of the hydrogen storage electrodes [33-41], because it allows to get an distinguishing of the different processes involved in the multi-step reactions. Most of the works have been using various electrical equivalent circuits for analyzing EIS spectra; despite the impedance spectra of the MH electrode are relatively similar. Moreover, the same EIS data can be analyzed with different electrical equivalent circuits [42,43]. Based on the study of impedance modeling of hydrogen storage electrodes, the unification of the equivalent model has not yet been achieved.

Nyquist diagrams of the $LaGaO_3$ working electrode measured at different cycles are depicts in Fig. 1. Each diagram contains two semicircles and an oblique line; a smaller loop in the high frequency region, a linear segment in the medium frequency and a larger loop in the low frequency region, reflecting the contact resistance between the current collector and the electrode particles, the Warburg semi-infinite diffusion impedance (W) [31,44-46] and the electrode surface process, respectively. The impedance spectrum of the LaGaO3 working electrode is relatively similar to that of other oxide-type electrodes $LaCrO_3$ [47] and $ZnFe_2O_4$ [48]. Song et al. [47] related the small semicircle in the high-frequency area of the $LaCrO_3$ oxide to mass-transfer process and the large semicircle to charge transfer resistance in the low frequency region. Zayani et al. [48] attributed the semicircle in the high-frequency area of the $ZnFe_2O_4$ ferrite to the charge-transfer process and the large semicircle of the low-frequency area to the electrode-surface processes.

The measured EIS data is fitted according to the proposed equivalent circuit shown in Fig.2, where R_s is the electrolyte resistance, R_u is the contact resistance between the current collector and the electrode particles, R_{ct} is the charge transfer resistance, R_{ht} is the hydrogen transfer resistance and W is the Warburg impedance. The constant phase element ($Q = CPE$)

is used in the equivalent circuit instead of capacitance taking into account the inhomogeneity and the roughness of the surface compound. The CPE impedance is estimated by [49-56]:

$$Z_{CPE} = \frac{1}{Y_{CPE}(j\omega)^n} \quad (1)$$

Where Y_{CPE} is the admittance; describes the non-perfect behavior of the capacitance (pseudo-capacitance), n is the CPE exponent, which satisfies $0 < n < 1$.

The impedance model fitted to the spectroscopy data with software ZSimpWin, as presented in Fig. 1, shows good fit quality. The objective of modeling is a minimization of the chi-square function χ^2, defined as:

$$\chi^2 = \sum_{\mathrm{i=1}}^{\mathrm{n}} \left[W_{\mathrm{i}}^{'} \left(Z_{\mathrm{i,exp}}^{'} - Z_{\mathrm{i,calc}}^{'} \left(\omega_{\mathrm{i}}, \overline{p} \right) \right)^2 + W_{\mathrm{i}}^{''} \left(Z_{\mathrm{i,exp}}^{''} - Z_{\mathrm{i,calc}}^{''} \left(\omega_{\mathrm{i}}, \overline{p} \right) \right)^2 \right] \quad (2)$$

Where $Z'_{\mathrm{i,exp}}(Z'_{\mathrm{i,calc}})$ and $Z''_{\mathrm{i,exp}}(Z''_{\mathrm{i,calc}})$ represent the real and imaginary parts of the experimental impedance (calculated), respectively, at the frequency ω_{i}, W_i' and W_i'' are the statistic weights data and n is the number of data points. The modeling was considered acceptable when, the chi-square function, $\chi^2 < 10^{-3}$ [57].

The parameter values of the model used above fitted by software ZSimpWin are reported in Table 1. The value of the electrolyte resistance (R_{s}) remains practically constant independently of cycling (R_{s}~0.33 $\Omega.cm^2$). The contact resistance R_{u} values characterize the electrical conductivity between the active material of the electrode and the nickel grid; the lowest value of R_{u} is observed over the first cycling, which is attributed to the good conductivity. Figure 3 illustrates the evolution of the charge transfer resistance R_{ct} as a function number of cycles. It can be found that R_{ct} values decreased during the first two cycles, from 1.77 Ω cm^2 (1$^{\mathrm{st}}$ cycle) to 1.44 Ω cm^2 (2$^{\mathrm{nd}}$ cycle), which indicates that the oxide has a better activation property. Then it gradually increased after activation to the value 2.41

Ω cm^2 (18th cycle). This behavior is also seen in conventional metal hydrides in previous studies and is ascribed to pulverization and oxidation of the MH electrode [58-60]. The value of R_{ct} is lower compared to that $ZnFe_2O_4$ spinel zinc ferrite and a little higher than $LaFeO_3$ perovskite oxide. Zayani et al. [48] showed that the charge transfer resistance of $ZnFe_2O_4$ oxide can reach 4.36 Ω cm^2 after activation. Pei et al. [61] reported that the calculated charge transfer resistance is 1.2 and 1 mΩ for untreated $LaFeO_3$ and carbon coated $LaFeO_3$ electrodes respectively, which were both prepared by polyaniline (PANI) pyrolysis method.

The pseudo-double layer capacitance CPE_{dl} was obtained by the following equation:

$$CPE_{dl} = (Y_{dl}R_{ct})^{1/n_{dl}}/R_{ct} \quad (3)$$

The CPE_{dl} values of the oxide gradually decreased with the first five cycles from 302.2 (1st cycle) to 194 μF cm^{-2} (5th cycle) and then increased (Fig. 4). The change of the electrode surface over cycling may be contributed to the variation of pseudo-double layer capacitance CPE_{dl}. With cycling, the electrode structure changed in various ways: agglomeration, roughening, and dissolution [62]. The exponent values of CPE_{dl} (n_{dl} *in Table* 1) are less than unity, varied between 0.54-0.89, indicating a strong modification in the surface of electrode with cycling. The *CPE* element Q_{dl} cannot represent the perfect capacitance when ($n_{dl} < 1$). The obtained CPE_{dl} value is very low compared to that reported in literature for $ZnFe_2O_4$ activated material which is 2.53 μF cm^{-2} [48]. The Warburg elememt Y_0 is related to the mass hydrogen diffusion. The fitted value of Y_0 also changed in the same way as CPE_{dl} (Table 1). The hydrogen diffusion rate is principally affected by the morphological and the structure change of the working electrode over cycling.

The current density I_0 which is generally used to describe the kinetics properties of the charge transfer reaction, is obtained by the following equation [63,64]:

$$I_0 = \frac{RT}{F}\frac{1}{mR_{ct}} \quad (4)$$

Where T, F, m, R and R_{ct} are the absolute temperature, the faraday constant (96500 C mol^{-1}), the effective mass of material, the gas constant and the charge-transfer resistance. The calculated I_0 of the $LaGaO_3$ oxide electrode is plotted in Fig. 5. The value of the exchange current increases rapidly during the activation process from 307.25 (1st cycle) to 377.67 mA g^{-1} (2nd cycle), and then decreases gradually after activation towards the value 225.66 mA g^{-1} (18th cycle). The pulverization of the electrode particles with cycling, which generates new surface area contact directly to KOH solution, leads to the corrosion of the electrode/electrolyte interface [65-67]. The result of I_0 is in good correlation with the value of charge transfer resistance R_{ct}. The calculated I_0 of the prepared oxide is higher with those found for traditional materials of the hydrogen battery [68-74]. Figure 6 illustrates the SEM images of the working oxide before and after cycling. Strong modification in the morphology of the oxide surface before and after electrochemical tests has been observed (Fig. 6). With cycling, the electrode powder is fractured and pulverized into a micro-sized grains due to the absorption/desorption of hydrogen. Generally, the pulverization of the electrode particles over cycling tends to facilitate the corrosion process. The average particle size of the oxide after cycling is about 39 μm.

The parameters R_{ht} and CPE_{ht} reflect the behavior of the hydrogen transfer process on the electrode surface. The fitted values of the hydrogen transfer resistance R_{ht} rapidly decreases during the activation process from 490 (1st cycle) to 10.32 Ω.cm^2 (2nd cycle), and then increases after activation towards the value 609.7 Ω.cm^2 (18th cycle) (Table 1).The larger value of R_{ht} before activation may be ascribed to the low-surface activity. The values of the pseudo-capacitance CPE_{ht}, calculated from the equation: $CPE_{ht} = (Y_{ht}R_{ht})^{1/n_{ht}}/R_{ht}$,

changed also in a same way as R_{ht}(Table 1). The variation of the CPE_{ht} could be attributed to the inhomogeneity surface of the oxide electrode, due to the modifications in the morphology and the microstructure of the electrode during cycling. The exponent values of $CPE_{\mathrm{ht}}(n_{\mathrm{ht}}\ in\ Table\ 1)$ varied between 0.86–0.99, which suggests that the CPE element Q_{ht} cannot represent the perfect capacitance. This behavior implies that the electrode surface is heterogeneous.

4. Conclusion

In this study, we investigated the influence of cycling on the kinetic characteristics of the working electrode $LaGaO_3$ using the EIS technique. A physicochemical model is proposed to analyzing the kinetic behavior of the oxide. The equivalent circuit showed excellent agreement with the spectroscopy data. The EIS results showed that the current density I_0 of the oxide increase quickly during the activation process and its maximum value is obtained at the second cycle (377.67 mA g^{-1}). The degradation of the current density after activation can be ascribed to pulverization and oxidation of the working electrode. A good correlation between Warburg impedance Y_0 and pseudo-double layer capacitance CPE_{dl} is observed. The variation of Y_0 may be explained by the change in the morphological and the structure of the working electrode over cycling. The EIS analysis relieved that electrochemical behavior of the oxide is controlled by the charge-transfer rate and the electrode surface.

In summary, the $LaGaO_3$ oxide electrode has good kinetic properties during the activation process. The exchange current of this oxide is higher with those found for some traditional materials of the hydrogen battery. Thus, $LaGaO_3$ can be employed new anode for Ni/MH batteries. However, the degradation of kinetic behavior needs to be further investigated after activation. The proposed solution may be is substituting La or Ga sites in the $LaGaO_3$ electrode to improve kinetic properties.

Data Availability Statement

The data that support the findings of this study are available from the corresponding author upon reasonable request.

Acknowledgements

The authors would like to thank the Deanship of Scientific Research at Umm Al-Qura University for supporting this work by Grant Code: (22UQU4331138DSR01).

References

1. Young K, Nei J, Huang B, Fetcenko MA. Studies of off-stoichiometric AB_2 metal hydride alloy: part 2. Hydrogen storage and electrochemical properties. Int J Hydrogen Energy 2011;36:11146-54

2. Rogulski Z, Dłubak J, Karwowska M, Krebs M, Pytlik E, Schmalz M, et al. Studies on metal hydride electrodes containing no binder additives. J Power Sources 2010;195:7517-7523

3. Li S, Zhao M, Wang L, Liu , Wang Y. Structures and electrochemical characteristics of $Ti_{0.26}Zr_{0.07}V_{0.24}Mn_{0.1}Ni_{0.33}Mo_x$ (x = 0–0.1) hydrogen storage alloys. Mater Sci Eng 2008;150:168-174

4. Miyamura H, Sakai T, Kuriyama N, Oguro K, Kato A, Ishikawa H. Hydrogen absorption and electrode characteristics of Ti–Zr–Ni–V–X alloys .Electrochem Soc Proc 1992;92-5:179-198

5. Mu D, Hatano Y, Abe T, Watanabe K. Degradation kinetics of discharge capacity for amorphous Mg–Ni electrode. J Alloys Compd 2002;334:232-37

6. Zhou Z, Song Y, Cui S, Huang C, Qian W, Lin C, Zhang Y, Lin Y. Effect of annealing treatment on structure and electrochemical performance of quenched $MmNi_{4.2}Co_{0.3}Mn_{0.4}Al_{0.3}Mg_{0.03}$ hydrogen storage alloy. J. Alloys Compd 2010;501:47-53.

7. Ma X, Wei X, Dong H, Liu Y. The relationship between discharge capacity of $LaNi_5$ type hydrogen storage alloys and formation enthalpy. J. Alloys Compd 2010;490:548-51.

8. Raju M, Ananth MV, Vijayaraghavan L.Influence of electroless coatings of Cu, Ni–P and Co–P on $MmNi_{3.25}Al_{0.35}Mn_{0.25}Co_{0.66}$ alloy used as anodes in Ni–MH batteries J. Alloys Compd 2009;475:664-71.

9. Nathira Begum S, Muralidharan VS, Ahmed Basha C, Electrochemical investigations and characterization of a metal hydride alloy ($MmNi_{3.6}Al_{0.4}Co_{0.7}Mn_{0.3}$) for nickel metal hydride batteries. J. Alloys Compd. 2009;467:124-29.

10. Kumar EA, Maiya MP, Murthy SS, Viswanathan B. Structural, hydrogen storage and thermodynamic properties of some mischmetal–nickel alloys with partial substitutions for nickel. J. Alloys Compd. 2009;47:92-97.

11. Li SL, Chen W, Chen DM, Yang K. Effect of long-term hydrogen absorption/desorption cycling on hydrogen storage properties of $MmNi_{3.55}Co_{0.75}Mn_{0.4}Al_{0.3}$. J. Alloys Compd. 2009;474:164-168.

12. Vivier V, Cachet-Vivier C, Nédélec J.-Y , Yu LT , Joubert JM , Percheron-Guégan A. Electrochemical study of $LaNi_{3.55}Mn_{0.4}Al_{0.3}Co_{0.75}$ by cavity microelectrode in 7 mol l^{-1} KOH solution. J Power Sources 2003;124:564-571

13. Khaldi C, Boussami S, Ben Rejeb B, Mathlouthi H, Lamloumi J. Corrosion effect on the electrochemical properties of $LaNi_{3.55}Mn_{0.4}Al_{0.3}Co_{0.75}$ and$LaNi_{3.55}Mn_{0.4}Al_{0.3}Fe_{0.75}$ negative electrodes used in Ni-MH batteries. Mater Sci Eng B 2010;175:22-28

14. Joubert J.-M, Cerny R, Latroche M., Percheron-Guegan A, Yvon K. Site occupancies in the battery electrode material $LaNi_{3.55}Mn_{0.4}Al_{0.3}Co_{0.75}$ as determined by multiwavelength synchrotron powder diffraction. J Appl Cryst, 1998;31:327-332

15. Dabaki Y, Khaldi C, ElKedim O, Fenineche N, i Lamloumi J. Structural, morphological, and electrochemical properties of AB_5 hydrogen storage alloy by mechanical alloying, Environ Prog Sustainable Energy. 2021:41: e13739

16. Dabaki Y, Khaldi C, ElKedim O, Fenineche N, Lamloumi J. Electrochemical properties of the $CaNi_{5-x}Mn_x$ electrodes synthesized by mechanical alloying. Int J Energy Res. 2020;44:10112-10125.

17. Dabaki Y, Khaldi C, ElKedim O, Fenineche N, Lamloumi J. Phase structure and electrochemical characteristics of $CaNi_{4.7}Mn_{0.3}$ hydrogen storage alloy by mechanical alloying, J Electrochem Soc. 2022:26:457–468

18. Chen M, Tan C, Jiang W, Huang J, Min D, Liao C, … Zhu M. Influence of over-stoichiometry on hydrogen storage and electrochemical properties of Sm-doped low-Co AB_5-type alloys as negative electrode materials in nickel-metal hydride batteries. J Alloys Compds, 2021:867:159111.

19. Chen X, Xu J, Zhang W, Zhu S, Zhang N, Ke D, Cheng H. Effect of Mn on the long-term cycling performance of AB5-type hydrogen storage alloy. Int J Hydrogen Energy. 2021:46(42): 21973–21983.

20. Zhang LL, Zhang WG, Zhu JW, Hao QL, Xu C, Yang XL, Lu LD, Wang X. Synthesis of $Er_2Ti_2O_7$ nanocrystals and its electrochemical hydrogen storage behavior.J Alloys Compd. 2009;480:L45–L48

21. Esaka T, Sakaguchi H., Kobayashi S. Hydrogen storage in proton conductive perovskite type oxides and their application to nickel-hydrogen batteries. Solid State Ionics 2004;166 :351-357

22. Deng G, Chen Y, Tao M, Wu C, Shen X, Yang H. Electrochemical properties of $La_{1-x}Sr_xFeO_3$ (x=0.2,0.4) as negative electrode of Ni–MH batteries. Electrochimica Acta 2009;54 :3910-3914

23. Mandal TK, Sebastian L, Gopalakrishnan J, Abrams L, Goodenough JB. Hydrogen uptake by barium manganite at atmospheric pressure. Mater Res Bull 2004;39:2257-2264

24. Deng G, Chen Y, Tao M, Wu C, Shen X, Yang H, Liu M. Preparation and electrochemical properties of $La_{0.4}Sr_{0.6}FeO_3$ as negative electrode of Ni/MH batteries. Int J Hydrogen Energy 2009;43:5568–5573

25. Lundqvist A, Lindbergh G. Kinetic study of a porous metal hydride electrode. Electrochim. Acta 1999;44:2523-2542

26. Yuan X, Xu N. Determination of hydrogen diffusion coefficient in metal hydride electrode by modified Warburg impedance. J. Alloys Compd 2001;329:115-120

27. Deng C, Shi P , Zhang S. Fabrication of bipolar nickel metal hydride batteries with nanometer copper oxide as anodic additive. Electrochim. Acta 2006 ;51:5349-5355

28. Kaabi A, Tliha M, Dhahri A, Khaldi C, Lamloumi J. Study of electrochemical performances of perovskite-type oxide $LaGaO_3$ for application as a novel anode material for Ni-MH secondary batteries, Ceramics International 2016;42:11682-11686

29. Mathlouthi H, Lamloumi J, Latroche M, Percheron-guegan A. Study of poly substituted intermetallic hydrides: electrochemical applications. Ann. Chim. Sci. Mater. 1997;22:241-244.

30. Geng M, Han J, Feng F, Northwood DO. Charging/discharging stability of a metal hydride battery electrode. J. Electrochem. Soc. 1999;146:2371-2375

31. Mathlouthi H, Khaldi C, Moussa MB, Lamloumi J, Percheron-Gu_egan A. Electrochemical study of mono-substituted and poly-substituted intermetallic hydrides. J Alloys Compds 2004;375:297-304.

32. Li CJ, Wang FR, Cheng WH, Li W, Zhao WT. The influence of high-rate quenching on the cycle stability and the structure of the AB_5-type hydrogen storage alloys with different Co content. J Alloys Compds 2001;315:218-223.

33. Lim C, Pyun SI. Theoretical approach to faradaic admittance of hydrogen absorption reaction on metal membrane electrode. Electrochim Acta 1993;38:2645-2652

34. Kuriyama N, Sakai T, Miyamura H, Uehara I, Ishikawa H, Iwasaki T. Electrochemical Impedance Spectra and Deterioration Mechanism of Metal Hydride Electrodes. J Electrochem Soc 1992;139:L72-L73

35. Zhang W, Kumar MPS, Srinivasan S, Ploehn HJ. AC Impedance Studies on Metal Hydride Electrodes. J. Electrochem Soc 1995;142:2935-2943

36. Wang C. Kinetic Behavior of Metal Hydride Electrode by Means of AC Impedance, J. Electrochem Soc 1998;145(6):1801-1812

37. Zheng G, Haran BS, Popov BN, White RE. Studies on metal hydride electrodes with different weights and binder contents. J. Appl Electrochem 1999;29:361-369

38. Deng C, Shi P, Zhang S. Effect of surface modification on the electrochemical performances of LaNi5 hydrogen storage alloy in Ni/MH batteries. Mater Chem Phys 2006;98:514-518

39. Wang Y, Lu ZW, Wang YL, Yan TY, Qu JQ, Gao XP, Shen PW. Electrochemical hydrogen storage of ball-milled CeMg12 and PrMg12 alloys with Ni powders. J Alloys Compd 2006;421:236-239

40. Gao X, Liu J, Ye S, Song D, Zhang Y. Hydrogen adsorption of metal nickel and hydrogen storage alloy electrodes. J Alloys Compd 1997;253: 515-519

41. Gao XP, Zhang W, Yang HB, Song DY, Zhang YS, Zhou ZX,Shen PW. Electrochemical properties of the $Zr(W_{0.4}Ni_{0.6})_{2.4}$ hydrogen storage alloy electrode. J Alloys Compd 1996;235: 225-231

42. Liu C, Bi Q, Leyland A, Matthews A. An electrochemical impedance spectroscopy study of the corrosion behaviour of PVD coated steels in 0.5 N NaCl aqueous solution: Part I. Establishment of equivalent circuits for EIS data modelling. Corrosion Science 2003;45:1243–1256.

43. Cui N, Luo JL. AC impedance study of self-discharge mechanism of nickel-metal hydride (Ni-MH) battery using Mg_2Ni-type hydrogen storage alloy anode. Electrochimica Acta 2000;45:3973–3981

44. Baddour-Hadjean R, Mathlouthi H., Pereira-Ramos JP, Lamloumi J, Latroche M, Percheron-Guegan A. ,An electrochemical study of mono-substituted intermetallic hydrides. J. Alloys Compd. 2003;356:750-754.

45. Xu YH, He GR, Wang XL. Hydrogen evolution reaction on the AB_5 metal hydride electrode. Int. J. Hydrogen Energy 2003;28:961-965

46. Khaldi C, Mathlouthi H, Lamloumi J. A comparative study, of 1 M and 8 M KOH electrolyte concentrations, used in Ni–MH batteries. J. Alloys Compd. 2009;469:464-471.

47. Song M, Chen Y, Tao M, Wu C, Zhu D, Yang H. Some factors affecting the electrochemical performances of LaCrO3 as negative electrodes for Ni/MH batteries. Electrochimica Acta 2010;55: 3103-3108

48. Zayani W, Azizi S, El-Nasser KS, Othman Ali I, Molière M, Fenineche N, Mathlouthi H, Lamloumi J. Electrochemical behavior of a spinel zinc ferrite alloy obtained by a simple sol-gel route for Ni-MH battery applications. Int. J. Energy Res. 2020: 45: 5235 -5247

49. Yuan XZ, Song C, Wang H, Zhang J. Electrochemical impedance spectroscopy in PEM fuel cells. New York: Springer; 2010.

50. Jorcin JB, Orazem ME, Pebere N, Tribollet B. CPE analysis by local electrochemical impedance spectroscopy. Electrochim. Acta 2006;51:1473-1479.

51. Sanchez M, Gregori J, Alonso C, Garcia-Jareno JJ, Takenouti H, Vicente F. Electrochemical impedance spectroscopy for studying passive layers on steel rebars immersed in alkaline solutions simulating concrete pores. Electrochim. Acta 2007;52:7634-7641.

52. Joiret S, Keddam M., Novoa XR, Perez MC, Rangel C, Takenouti H. Use of EIS, ring-disk electrode, EQCM and Raman spectroscopy to study the film of oxides formed on iron in 1 M NaOH. Cem. Concr. Compos 2002;24:7-15.

53. Chen WX. Effects of surface treatments of $MlNi_{4.0}Co_{0.6}Al_{0.4}$ hydrogen storage alloy on the activation, charge/discharge cycle and degradation of Ni/MH batteries. J. Power Sources 2001;92:102-107.

54. Boukamp BA. Electrochemical impedance spectroscopy in solid state ionics: recent advances. Solid State Ionics 2004;169:65-73.

55. Liu W, Wub H, Lei Y, Wang Q. Reaction kinetics of amorphous $Mg_{50}Ni_{50}$ hydride electrode. J. Alloys Compd. 2002;346:244-249.

56. Cui N, Luo JL, Chuang KT. Nickel–metal hydride (Ni–MH) battery using Mg_2Ni-type hydrogen storage alloy. J. Alloys Compd. 2000;302:218-226

57. Cui XY, Martin DC. Electrochemical Deposition and Characterization of Poly (3,4-Ethylenedioxythiophene) on Neural Microelectrode Arrays, Sens Actuators B Chem., 2003;89:92–102

58.Chen W. Effects of surface treatments of $MlNi_{4.0}Co_{0.6}Al_{0.4}$ hydrogen storage alloy on the activation, charge/discharge cycle and degradation of Ni/MH batteries. J Power Sources 2001; 92:102-107

59. Geng M, Feng F, Sebastian PJ, Matchett AJ, Northwood DO. Charge transfer and mass transfer reactions in the metal hydride electrode. Int J Hydrogen Energy 2001;26:165-169.

60. Tsai PJ, Chiu T.C., Tsai PH, Lin KL, Lin KS, Chan SLI. Carbon nanotube buckypaper/MmNi5 composite film as anode for Ni/MH batteries. Int J Hydrogen Energy 2012;37:3491-3499.

61. Pei Y, Li Y, YinghuiChe J, Shen W, Wang Y, Yang S, Han S, Study on the high-temperature electrochemical performance of perovskite-type oxide $LaFeO_3$ with carbon modification, Int J Hydrogen Energy 2015:40:8742-8749

62. Darab M, Dahlstrøm PK, Thomassen MS, Seland F, Sunde S. Dynamic electrochemical impedance spectroscopy of Pt/C-based membrane-electrode assemblies subjected to cycling protocols. Journal of Power Sources 2013;242:447-454

63. Notten PHL, Hokkeling P. Double-Phase Hydride Forming Compounds: A New Class of Highly Electrocatalytic Materials. J Electrochem Soc. 1991;138:1877–1885

64. Pan H, Liu Y, Gao M, Zhu Y, Lei Y, Wang Q. A study on the effect of annealing treatment on the electrochemical properties of $La_{0.67}Mg_{0.33}Ni_{2.5}Co_{0.5}$ alloy electrodes. Int J Hydrogen Energy 2003;28:113–117.

65. Ruggeri S, Roue L. Correlation between charge input and cycle life of MgNi electrode for Ni-MH batteries. J Power Sources 2003;117:260-266.

66. Luo JL, Cui N. Effects of microencapsulation on the electrode behavior of Mg2Ni-based hydrogen storage alloy in alkaline solution. J Alloys Comp 1998;264:299-305.

67. Liu Y, Pan H, Yue Y, Wu X, Chen N, Lei Y. Cycling durability and degradation behavior of La-Mg-Ni-Co-type metal hydride electrodes. J Alloys Comp 2005;395:291-299

68. Yuan A, Xu N. A study on the effect of nickel, cobalt or graphite addition on the electrochemical properties of an AB_5 hydrogen storage alloy and the mechanism of the effects. J Alloys Compd. 2001;322:269–275

69. Verbetsky VN, Petrii OA, Vasina SY, Bespalov AP. Electrode materials based on hydrogen-sorbingalloys of AB_2 composition (A = Ti, Zr; B = V, Ni, Cr). Int J Hydrogen Energy 1999;24:247–249

70. Zhang X, Yin W, Chai Y, Zhao M. Structure and electrochemical characteristics of $RENi_3$ alloy. Mater Sci Eng B 2005;117:123–128

71. Shi Y, Leng H, Wei L, Chen S, Li Q. The microstructure and electrochemical properties of Mn-doped La-Y-Ni-based metal-hydride electrode materials. Electrochimica Acta 2019 ;296:18-26

72. Wan C, Denys RV, Lelis M, Milčius D, Yartys VA. Electrochemical studies and phase-structural characterization of a high-capacity La-doped AB_2 Laves type alloy and its hydride. J Power Sources 2019;418:193-201

73. Wang Q, Chao D, Zhou W, Chen Y, Wu C. Influence factors of capacity loss after short-time standing of metal-hydride electrode and its EIS model. Journal of Rare Earths 2013;31:772-777

74. Han J, Feng F, Geng M, Buxbaum R, Northwood D O. Electrochemical characteristics of the interface between the metal hydride electrode and electrolyte for an advanced nickel/metal hydride battery. J Power Sources 1999;80:39-45,

Figure captions

Fig.1. Experimental spectra of the oxide electrode at different cycles, compared with model fit: (a) cycle1, (b) cycle2, (c) cycle5, (d) cycle12 and (e) cycle18.

Fig.2. Equivalent circuit of the $LaGaO_3$ anode material.

Fig.3. The charge transfer resistance R_{ct} value vs. cycles

Fig.4. The pseudo-double layer capacitance CPE_{dl} value vs. cycles

Fig.5. The exchange current density I_0 value vs. cycles

Fig.6. SEM photograph of the working oxide: (a) before cycling; (b) after cycling.

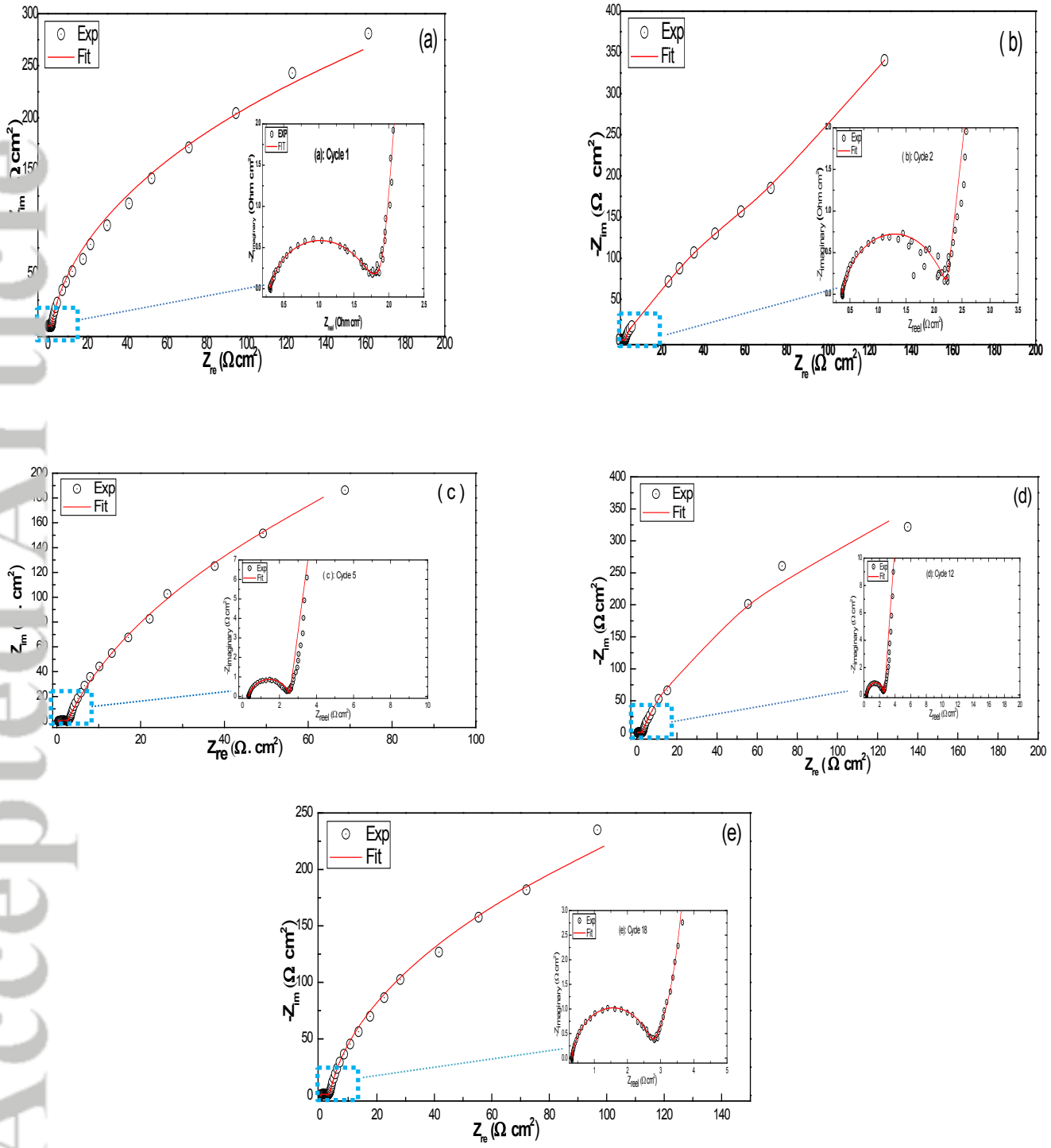

Fig.1. Experimental spectra of the oxide electrode at different cycles, compared with model fit: (a) cycle1, (b) cycle2, (c) cycle5, (d) cycle12 and (e) cycle18.

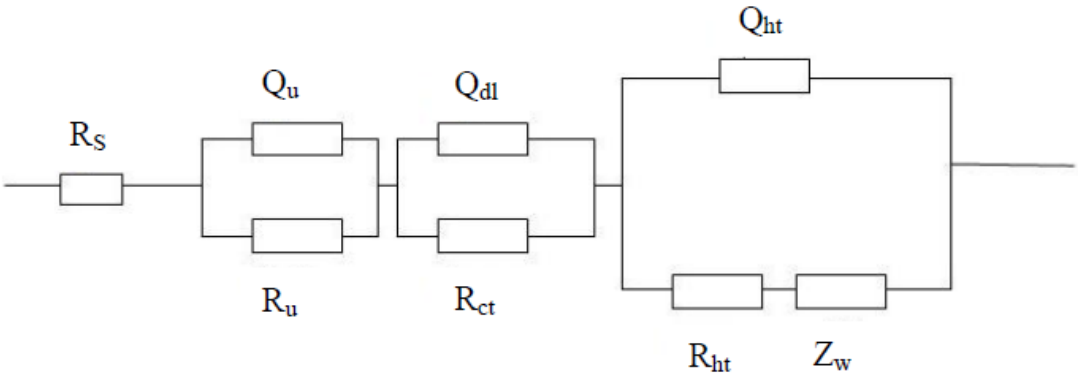

Fig.2. Equivalent circuit of the $LaGaO_3$ anode material.

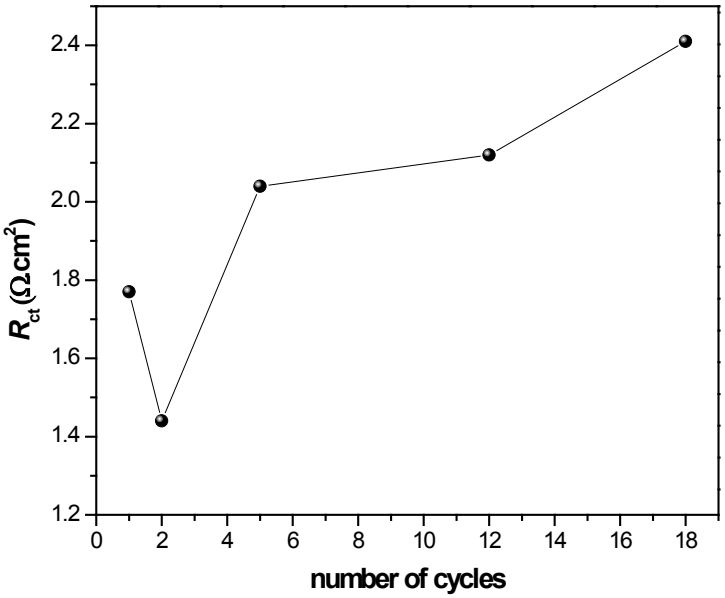

Fig.3. The charge transfer resistance R_{ct} value vs. cycles.

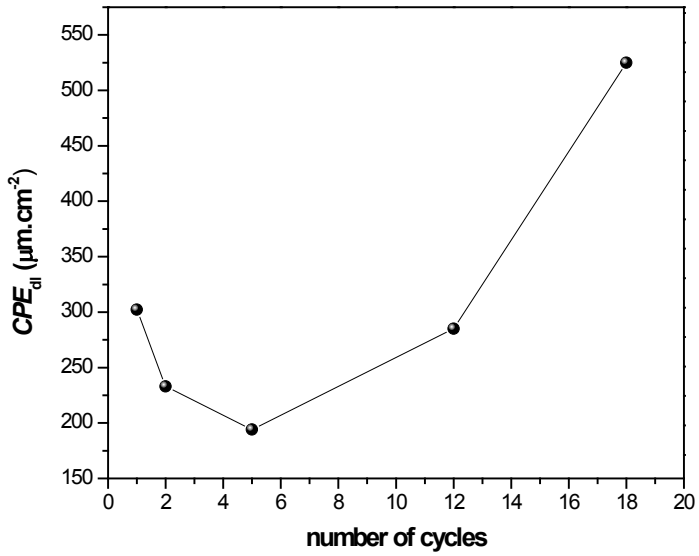

Fig.4. The pseudo-double layer capacitance CPE_{dl} value vs. cycles.

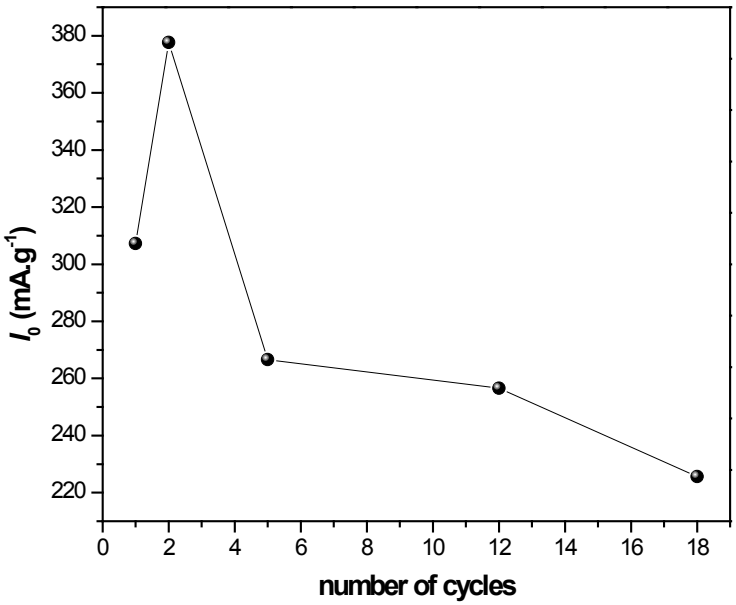

Fig.5. The exchange current density I_0 value vs. cycles.

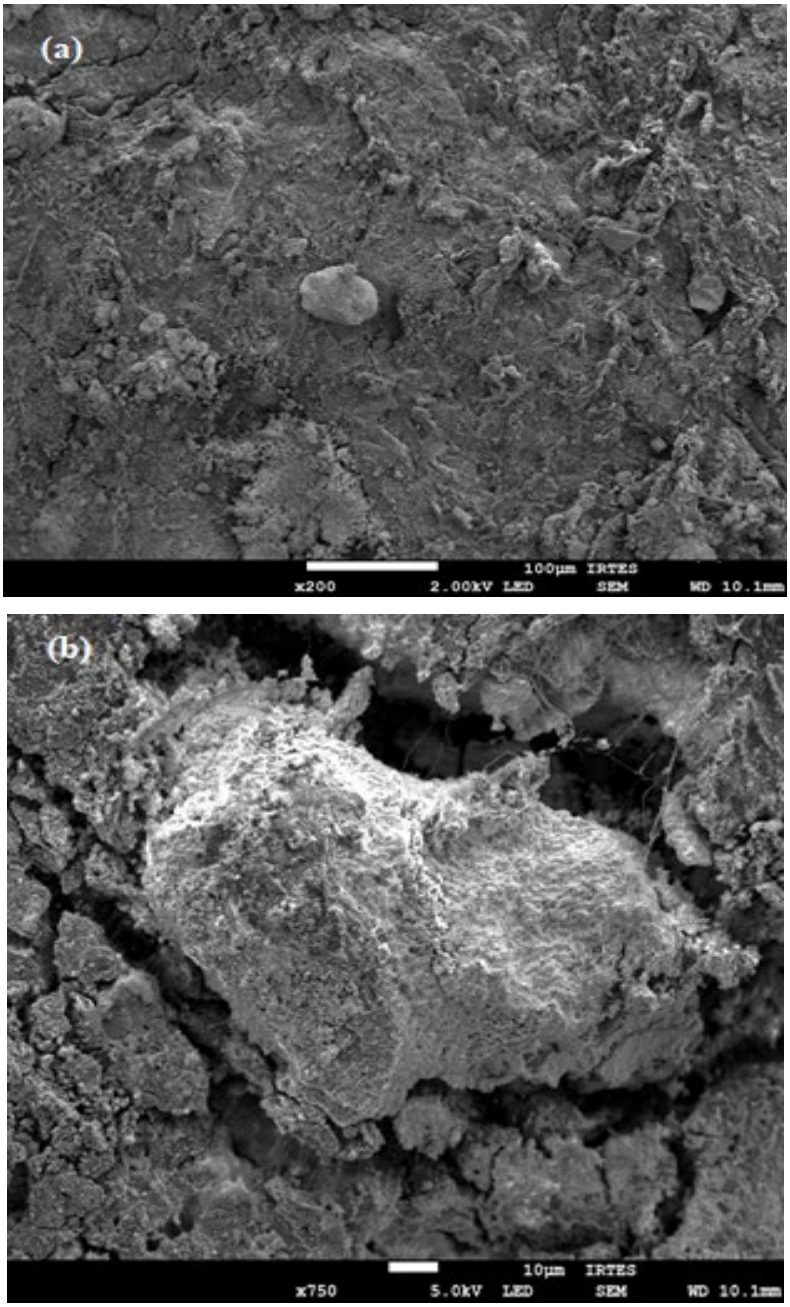

Fig.6. SEM photograph of the working oxide: (a) before cycling; (b) after cycling.

Table captions:

Table.1: Values of fitting parameters of the $LaGaO_3$ oxide electrode.

Parameters	cycle 1	Cycle2	Cycle5	Cycle12	Cycle18
R_S (Ω cm^2)	0.30	0.36	0.33	0.34	0.32
R_u (Ω cm^2)	0.38	0.39	1.99	1.15	0.99
Q_u, Y_u (F cm^2)	0.222	0.00592	0.00059	0.51	0.432
Q_u, n_u	0.5	1	0.88	0.56	0.71
R_{ct} (Ω cm^2)	1.77	1.44	2.04	2.12	2.41
Q_{dl}, Y_{dl} (mF cm^{-2})	0.678	0.55	0.59	0.671	1.133
Q_{dl}, n_{dl}	0.89	0.89	0.54	0.88	0.88
R_{ht} (Ω cm^2)	490	10.32	400.2	328.8	609.7
Q_{ht}, Y_{ht} (F cm^{-2})	0.309	0.29	0.306	0.33	0.296
Q_{ht}, n_{ht}	0.99	0.86	0.96	0.97	0.95
Z_w, Y_0 (S s$^{0.5}$ cm^{-2})	0.058	0.03	0.033	0.036	0.078
CPE_{dl} (μF cm^{-2})	302.2	233	194	285	525
CPE_{ht} (mF cm^{-2})	324.9	115.47	370.86	379.8	383.8
I_0 (mA g^{-1})	307.25	377.67	266.59	256.53	225.66
$\chi^2\times10^{-4}$	9.84	2.00	1.73	5.43	1.96